RADIO SCIENCE, VOL. 48, 197–207, doi:10.1002/rds.20023, 2013

# The processing of electron density profiles from the Mars Express MARSIS topside sounder

D. D. Morgan,[1] O. Witasse,[2] E. Nielsen,[3] D. A. Gurnett,[1] F. Duru,[1] and D. L. Kirchner[1]

Received 6 July 2012; revised 18 January 2013; accepted 4 February 2013; published 15 May 2013.

[1] We here present a manual for the reduction of data from ionograms obtained from the Mars Express MARSIS Active Ionospheric Sounding topside radar sounder. Sample data are presented with the procedure for processing them explained as simply as possible. We discuss the uncertainties inherent in the measurements as well as systematic problems with the data. A sample code is included to facilitate the inversion process. We also include a comparison with an electron density profile taken from the Mars Express Radio Science occultation experiment, showing agreement between the two methods, although the data are not simultaneous.

**Citation:** Morgan, D. D., O. Witasse, E. Nielsen, D. A. Gurnett, F. Duru, and D. L. Kirchner (2013), The processing of electron density profiles from the Mars Express MARSIS topside sounder, *Radio Sci.*, *48*, 197–207, doi:10.1002/rds.20023.

## 1. Introduction

[2] The recent public availability of ionogram data from the Active Ionospheric Sounding (AIS) mode of the Mars Advanced Radar for Subsurface and Ionosphere Sounding (MARSIS) instrument, on board the ESA Mars Express spacecraft, has created an interest, among researchers in the Mars Express community and beyond, in learning about the processes used to analyze topside sounder ionograms. This document is intended as a ready reference to enable researchers inexperienced in the theory and practice of ionogram inversion to make use of the mass of data currently becoming available. The authors all have experience in the processes of acquiring the required data and inverting them to obtain the electron density profile. This document comprises seven sections, including this Introduction (section 1). Section 2 discusses the basic structure of the MARSIS ionogram data. Section 3 discusses how the electron density at the spacecraft is obtained from harmonics of plasma oscillations in the plasma around the spacecraft. Section 4 discusses the acquisition of the ionospheric trace, or "delay time" as a function of sounding frequency. Section 5 discusses processing of the trace, in particular, removal of data points corrupted by noise. Section 6 discusses how the ionospheric trace is inverted to give the electron density as a function of altitude, i. e., the vertical electron density profile. Section 7, the final section, is a summary of any caveats or pitfalls that exist in this process along with a comparison with a Mars Express Radio Science occultation profile.

[1]Department of Physics and Astronomy, University of Iowa, Iowa City, Iowa, USA.
[2]Research and Scientific Support Department of the European Space Agency, ESTEC, Noordwijk, The Netherlands.
[3]Max Planck Institute for Solar System Research, Katlenburg-Lindau, Germany.

Corresponding author: D. D. Morgan, Department of Physics and Astronomy, University of Iowa, Iowa City, IA, USA. (david-morgan@uiowa.edu)


0048-6604/13/10.1002/rds.20023

[3] The archived MARSIS AIS data are available through the European Planetary Science Archive (PSA) at URL www.rssd.esa.int or through the U. S. Planetary Data System (PDS) at URL pds.nasa.gov.

## 2. Introduction to MARSIS Topside Ionospheric Sounding Data

[4] An ionospheric sounder works by transmitting a short electromagnetic pulse at near constant frequency and then "listening" for a possible reflected wave from the ionosphere or other object of interest. The use of electron magnetic sounding techniques to probe the ionosphere goes back to the mid-1920s, when ground-based sounders called "ionosondes" were first used to explore the bottomside of the Earth's ionosphere [*Reinisch*, 1996; *Benson*, 2010].

[5] Sounders designed to work above the main layer of the ionosphere are referred to as "topside" sounders. Ionospheric sounders are usually designed to extract density information from the plasma by utilizing a "swept frequency" design [*Franklin and Maclean*, 1969]. The first spacecraft-borne topside sounder was launched into Earth orbit in 1961 [*Benson*, 2010]. The Alouette and ISIS series were landmark topside sounders that yielded massive datasets that are still in use today [*Benson and Bilitza*, 2009]. The history and design of swept-frequency topside sounders is reviewed by *Franklin and Maclean* [1969] and by *Benson* [2010]. The design of both subsurface and ionospheric modes of the MARSIS sounder is documented by *Jordan et al*. [2009].

[6] The smallest unit of data that can be used to obtain a vertical electron density profile from the MARSIS ionospheric sounder is referred to as an ionogram. An ionogram consists of an array of received power plotted as a function of the sampled sounding frequencies and delay times. An example of an ionogram is shown in Figure 1. The *x*-axis corresponds to the sounding frequency. The left-hand *y*-axis gives the delay time, or time elapsed from the sounding pulse to sampling of the return signal. The right-hand y-axis gives the apparent range, i. e., the calculated range from the spacecraft assuming propagation at the speed of light, i. e., with no correction for

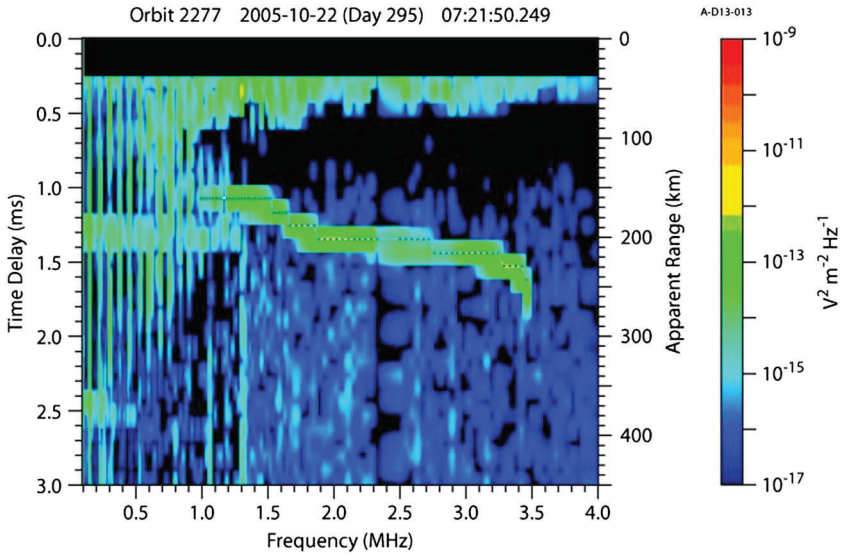


**Figure 1.** An ionogram from MARSIS AIS, with received intensity (color code) plotted against sounding frequency (*x* axis) and delay time (left-hand *y* axis) or apparent range from the spacecraft (right-hand *y* axis). Vertical lines in the upper left-hand corner are harmonics of the spacecraft-local plasma frequency due to distortion effects in the receiver. The mostly horizontal structure centered in the figure marked with a dotted line is the ionospheric echo. As discussed in the text, the "stairstep" effect of the ionospheric echo is due to the 91.4 μs resolution of the time delay (13.8 km resolution in apparent range).

dispersion caused by the intervening plasma. The values color-coded in the plot are the intensity of the received signal. The descending bright line centered in the figure is the sounding echo from the Martian ionosphere, the principal objective of ionospheric sounding. In addition to the sounding echo, there are vertical bright lines at low frequencies in the upper left corner of the ionogram. These bright lines are the result of an instrumental effect that produces harmonics of the plasma frequency local to the Mars Express spacecraft, a measurement that we shall find useful. We shall discuss the use of these locally generated signals in subsequent sections.

[7] In the normal MARSIS Active Ionospheric Sounding (AIS) mode of operation, 160 sounding frequencies ranging from 0.1 to 5.5 MHz are selected for optimum coverage. The sounding frequencies chosen underwent revision several times early in the mission to optimize coverage at frequencies below about 2 MHz and to avoid frequencies with high levels of interference. It was found that sampling at low frequency is at a premium because it is in this frequency range that the altitude of the ionosphere changes rapidly with plasma density, and also because the power of transmission of the sounding wave falls off abruptly with decreasing frequency. A quasi-logarithmic spacing of frequencies was found to optimize coverage in the low-frequency range. Figure 2 shows the difference between adjacent sounding frequencies as a function of the sounding frequency. Deviation from the overall stepwise pattern evident in Figure 2 was instituted to avoid sampling frequencies strongly contaminated with interference. The error bars indicate the bandwidth of the frequency sample, which is constant at 10 kHz. Figure 3 shows the spacing of the sounding frequencies normalized by the sounding frequency. This figure shows that, for frequencies greater than about 500 kHz, the frequency spacing is less than 5% of the frequency and that the average fractional spacing is about 2%. The final and current frequency table, which has

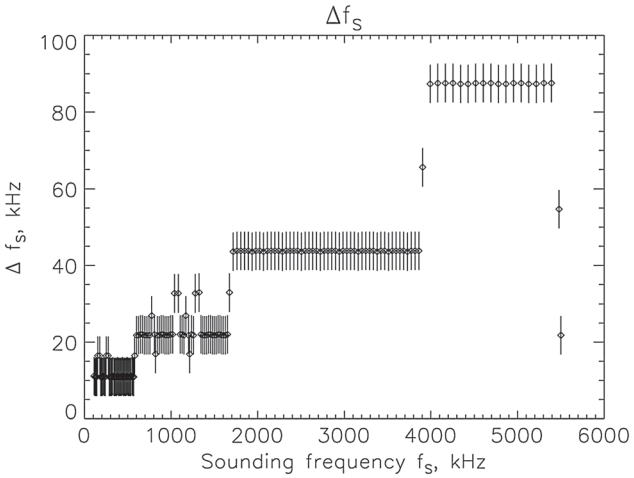


**Figure 2.** The MARSIS AIS sounding frequency table (*x* axis) and frequency spacing (*y* axis). The error bars are ± **5** kHz, the bandwidth of the measurement.

been in effect since 14 August 2005, can be accessed at the following web site: http://www-pw.physics.uiowa.edu/marsx/DOCUMENT/AIS_FREQ_TABLE.TXT.

[8] The sampled delay times measured from the start time of the sounding pulse at a given frequency are given by the formula

$$\begin{aligned} t_{\text{delay}} = {} & 91.4\,\mu\text{s} \ \ (\text{length of sounding pulse}) \\ & +162.5\,\mu\text{s} \ \ (\text{receiver dead time}) \\ & +i\cdot 91.4\,\mu\text{s} \ \ (\text{sampled delay times}), \ \ 0\le i\le 79 \end{aligned} \tag{1}$$

where the sampled times range from 253.9 to7565.9 μs. The first line of the right-hand side of Equation 1 is the length of the transmitted sounding pulse. Times are measured from the

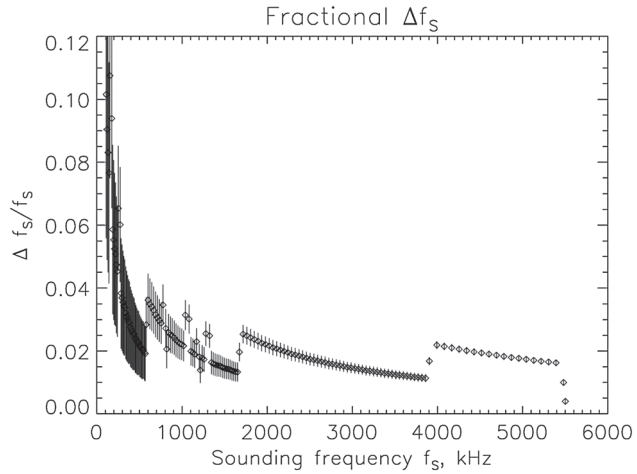


**Figure 3.** The MARSIS AIS sounding frequency table (*x* axis) and fractional frequency spacing (*y* axis). The error bars are $\pm$ 5 kHz/$f_s$, the bandwidth of the measurement normalized by the sounding frequency $f_s$.

start time of the sounding pulse. The second line of Equation 1 is the time interval during which neither transmission nor receiving is operating; this is referred to as "dead time". The purpose of dead time is to protect the receiver from immediately responding to the sounding wave, which is very intense and could damage the receiver. The third line of Equation 1 represents the 80 sample intervals of 91.4 μs each. The delay time is measured from the beginning of the sounding pulse to the beginning of each sample time. After the sampling sequence, there is another small dead time of 278 μs. This cycle takes 7.867 ms. It is then repeated at the next sampled frequency. The cycle of 80 frequencies takes 1.26 s. The instrument is then silent for five periods of 1.26 s, after which the cycle begins again. The entire data collection cycle takes 7.543 s.

## 3. The Local Plasma Frequency

[9] In the processing of an ionospheric trace, the corrected range for each data point is dependent on the plasma density profile of the ray path previously traversed by the sounding wave. In the case of a topside sounder, this implies that the plasma density at the spacecraft, referred to here as the *local* plasma density, provides the starting point for the entire calculation of an electron density profile and is therefore an essential piece of information. In this section, we show the method by which the local electron plasma frequency can in many cases be obtained.

[10] One of the early discoveries from MARSIS was that the instrument often recorded harmonics of the plasma oscillations occurring close to the spacecraft [see e. g., *Gurnett et al*., 2005]. There is a large literature on the detection by radar sounders of "resonances" of the local plasma and cyclotron frequencies, Bernstein modes, and other modes [*McAfee*, 1969; *Muldrew*, 1972; *Benson*, 2008]. In addition, the "relaxation sounder" is specially designed to detect locally stimulated oscillations. Examples of this type of sounder are the WHISPER sounder on board the four Cluster spacecraft [*Décréau et al*., 2001] and the sounder incorporated into the Radio and Plasma Wave Investigation on board the Cassini spacecraft [*Gurnett et al*., 2004]. Relaxation sounders are tuned to receive at frequencies corresponding to the local plasma and cyclotron frequencies at the position of the spacecraft.

[11] The MARSIS AIS instrument was primarily designed for remote sounding in the range 0.1–5.5 MHz. The sounding pulse is precisely tuned to the preset transmission frequency, but because the pulse is designed as a square wave, there are far-reaching sidebands. It is these sidebands, spaced at frequency intervals of $1/\Delta t_{\text{pulse}} = 1/91.4$ μs = 10.9 kHz, that put energy into plasma oscillations when the plasma frequency is well below the transmission frequency. Because the transmitted signal is quite strong (400 V), and the antenna is sensitive to signals as low as a microvolt, the plasma oscillations create a strong signal on the antenna that is fed to the receiver. These oscillations have higher amplitude than the range of the receiver and are therefore clipped, causing integer harmonics of the plasma frequency to resonate in the receiver. These harmonics, which are visible in Figure 4 as vertical high-intensity stripes, are easily exploited by measuring their average frequency separation to make a reasonably accurate measurement of the plasma frequency in the vicinity of the spacecraft. In Figure 4, the plasma frequency is measured to be 0.075 MHz. Note that the bright band corresponding to the actual plasma frequency is not visible on this ionogram. The method of taking the difference between the harmonic bands allows us to measure the plasma frequency even when it is somewhat below the smallest sampled frequency. These measurements are very useful as an independent data set and have been so used in a number of studies [see, e. g., *Duru et al*., 2008; *Duru et al*., 2010a]. In this manual, we discuss their contribution to the acquisition of electron density profiles.

[12] Many references, for example, [*Franklin and Maclean*, 1969; *Muldrew*, 1972; *Benson*, 2008], have discussed the existence of resonances in topside ionograms. In these papers, the resonance is inferred to be a ray that propagates obliquely and is reflected back to the antenna from tiny fluctuations in the ambient plasma density. We do not believe that this mechanism is the explanation of the plasma frequency resonances seen by MARSIS, since the spacecraft travels only 30 m in the 7.5 ms duration of a receive sweep for a single frequency, a distance less than the length of the MARSIS antenna. It seems clear that, in this range, direct excitation of oscillations at the plasma frequency should predominate over oblique reflection of propagating waves over distances on the order of 10 km. In addition, reflection over such a large range should result in Doppler broadening of the return signal, an effect that we do not see. We therefore believe that direct excitation of plasma oscillations in the immediate vicinity of the spacecraft is the correct explanation of the observed resonances.

[13] A reasonable estimate of the uncertainty in the spacecraft-local plasma frequency can be made by referring to Figure 3. The spacing between sampling frequencies at frequencies below 0.7 MHz (about the upper limit of the measured plasma frequency) varies between about 2 and 10%. The upper limit uncertainty comes to about 4% if the number of harmonic lines in the sample is treated as if it were the number of independent samples.

[14] Figure 5 illustrates one of the ambiguities of using plasma frequency harmonics to determine the local plasma frequency. In this figure, there is a set of bright plasma harmonics and a set of fainter harmonics occurring halfway between the bright ones. If the bright lines are used to indicate

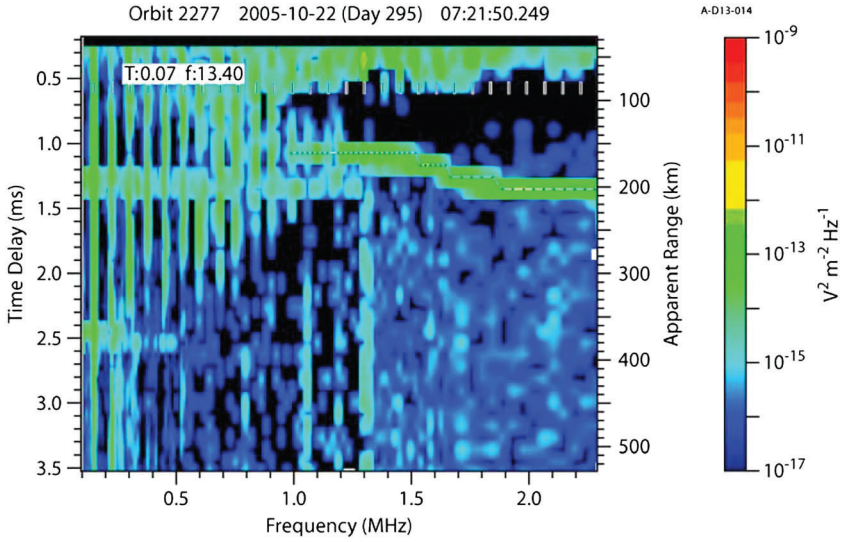


**Figure 4.** An expanded portion of Figure 1. The frequencies of the plasma oscillation frequencies are indicated by the short dark lines coinciding with the bright vertical bands. The best way to measure the local plasma frequency is to find the average difference in frequency between these harmonics. The plasma frequency in Figure 1 is measured to be 0.075 MHz. The first visible band in the figure, at about 0.15 MHz, is therefore at twice the plasma frequency. The ionospheric trace, measured using an intensity threshold, is shown as a white and black dotted line.

the plasma oscillation harmonics, the plasma frequency is measured as 0.625 MHz; if the fainter lines are included, the plasma frequency will be very nearly half of that. The probable explanation of the faint lines occurring at equally spaced intervals between the bright lines is that the signal, which is greater than the capacity of the receiver, is asymmetrically clipped, causing interspersed bright and faint lines. Thus, when bright and faint lines are interspersed at equal frequency intervals, both bright and faint lines should be taken into account.

[15] Sometimes it occurs that the lines are not evenly spaced. In this case, it is quite likely that the spacecraft passing through regions in which the density goes through a transition on a shorter distance scale than the motion of the spacecraft. Such an occurrence is quite possible because the spacecraft is traveling at approximately 4 km/s at altitudes where data are being taken, which translates to a distance of about 30 km in the 7.543 s between ionograms, or about 5 km in the 1.26 s it takes to collect data for a single ionogram. When the various sets of bright lines cannot be reconciled, one can examine the ionograms immediately before and after the ionogram in question for consistency. Unfortunately, it is sometimes inherently unclear which set of lines is correct. The detection of a changing plasma frequency over the

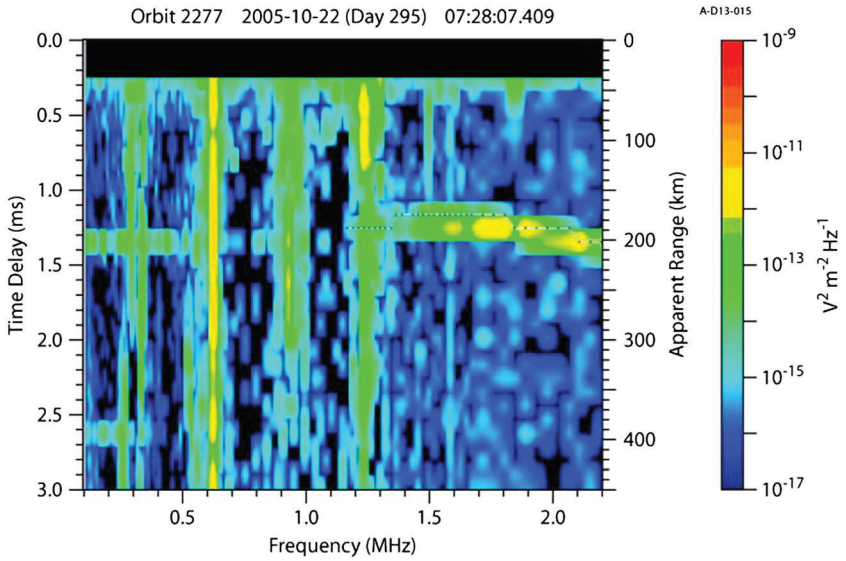


**Figure 5.** The plasma frequency is measured from the frequency difference between the bright vertical bands to be 0.625 MHz. Using the faint lines with the bright lines gives a result of 1/2 of that.

duration of a single ionogram has been observed at Earth by the Alouette 2 radar, as discussed by [*Benson*, 1985].

[16] There are times when the plasma oscillation harmonics are not available, as for example, when the spacecraft is in the shocked solar wind, where the excited wave packet is convected away from the spacecraft before it can be detected [*Duru et al*., 2008]. In such cases, the best independent guess of the plasma frequency at the spacecraft is usually the best that can be done. A value interpolated from surrounding measurements is a possibility that should be used with caution because of the inherent variability of the measurement. If the spacecraft is in the solar wind, the local plasma frequency can be independently estimated with some justification: a typical value of the solar wind density at the orbit of Mars is 3.8 $cm^{-3}$, corresponding to a plasma frequency of 0.018 MHz [*Duru et al*., 2008; *Schunk and Nagy*, 2000].

## 4. The Ionospheric Trace

[17] In this section, we shall describe the process for taking the ionospheric trace, i. e., acquiring the delay time of the sounding wave reflected from the ionosphere as a function of the sounding frequency. To start, we should note that this activity is the greatest contributor to uncertainty in the final result. The uncertainty in the local plasma frequency is typically 3% or less, while uncertainty in the elements of the trace is one pixel $= R_{app} = c \times t_{delay}/2 = (3 \times 10^5 km/s) \times (91.4\ \mu s)/2 = 13.7$ km or $\pm$ 6.9 km, which is approximately 10% of the ionospheric peak altitude. In addition to the inherent uncertainty in the measurement of delay time, the lower frequency limit on the visibility of the trace can seriously compromise the accuracy of the resulting electron density profile. This problem occurs because the sharp fall-off in transmitted power inherent in a dipole antenna usually causes frequencies below about 1 MHz to be undetectable. In reducing topside ionograms taken at Earth, use of the X-mode trace mitigates this problem because the X-mode has a higher-frequency cutoff due to the contribution of the magnetic field [*Jackson*, 1969]; at Mars, the magnetic field is weak enough that the X-mode is nonexistent, making this method irrelevant. To compound the problem at low frequencies, the signal is often swamped by noise. Because of the difficulties in taking reliable traces at low frequency, we have not attempted automatic processing of ionospheric traces. The trend now appears to be toward automation of detection and tracing of the ionospheric echo. For example, an algorithm using predictive sampling of ionograms has recently been demonstrated by [*Wang and Ping* [2012] to recover ionospheric traces with an estimated efficiency of 90%. However, the most generally accessible method remains direct manual scaling. Therefore, in this manual, we shall describe the simplest method for a person sitting at a computer screen using display software that includes a readable cursor.

[18] Another small source of error is that the transmitted sounding wave has a small but measureable rise-time, as shown in Figure 6. This figure shows the history of the transmitted voltage pulse on the antenna for a sampling of frequencies as measured in the engineering laboratory and captured on an oscilloscope screen. At all frequencies, the wave is at over half its final amplitude after approximately 3 μs, which translates to an error of about 0.45 km in apparent range. Since one pixel represents an uncertainty of $\pm$ 6.9 km, this effect is negligible.

[19] As noted above, and as is visible in Figure 1, the ionospheric reflection as seen on an ionogram has a finite width. Because the zero of the time measurement is the beginning of the transmitted sounding pulse, ideally one would take the measurement of the reflected trace at the leading edge of the reflection. However, because the worker is using an averaged ionogram displayed on a computer screen, the visual upper limit of the trace is likely to be too short an estimate.

[20] Two conventions have been used to determine the time delay. One method is to choose a threshold value of the intensity to define the upper edge of the ionospheric reflection. This value must be chosen empirically and is therefore somewhat arbitrary. This method also suffers from a slight bias along the trace because the reflected intensity decreases at low frequencies. This bias is always less than the inherent measurement error of $\pm$ 6.9 km and is therefore always neglected. A better-defined marker is the uppermost maximum intensity value of the ionospheric reflection. In practice, because of the rather coarse resolution in time delay, the threshold and maximum methods agree roughly half the time. When they disagree, the maximum method gives a value that is longer by one pixel = 91.4 μs. Because the two methods give results that are very close, the choice of criterion for determination of the trace position will largely be a matter of convenience depending on the software available to the worker. If digital values of the intensity are available, it is easy to use a threshold criterion. If the traces are made on the basis of a visual determination of brightness, then the trace maximum provides a more consistent standard. If one uses the maximum brightness as the tracing criterion, it can be reconciled on average with the results of the threshold method by subtracting 1/2 – pixel- or 45.7 μs, from each delay time. This correction is equivalent to treating the center time of the transmitted pulse as the zero time. Because this error is half of the pixel resolution, it is not usually considered necessary.

[21] In Figure 1, the ionospheric trace is made using a threshold of $1 \times 10^{-15} (V/m)^2/Hz$. It can be seen that in most cases this threshold is in the visual center of the reflection and close to the position of maximum brightness of the trace. A procedure for taking the trace is as follows:

1. Display desired ionogram on a computer monitor.
2. Determine the lowest frequency where the ionospheric trace is distinguishable from noise.
3. Use the cursor to digitize delay times for all sampled frequencies by either the threshold or maximum intensity method depending on available facilities.

[22] The resulting data consist of a list of sounding frequencies with corresponding delay times. These data will serve as input to the smoothing and inversion phases of the electron density profile process.

## 5. Processing of the Ionospheric Trace

[23] It has been noted that MARSIS ionograms are typically noisy at frequencies below 1 MHz. In particular, there are several strong interference frequencies that will corrupt the digitized trace in the case where an automated procedure is used to do the measurement. A trace done by an automated method must always be examined for corruption due

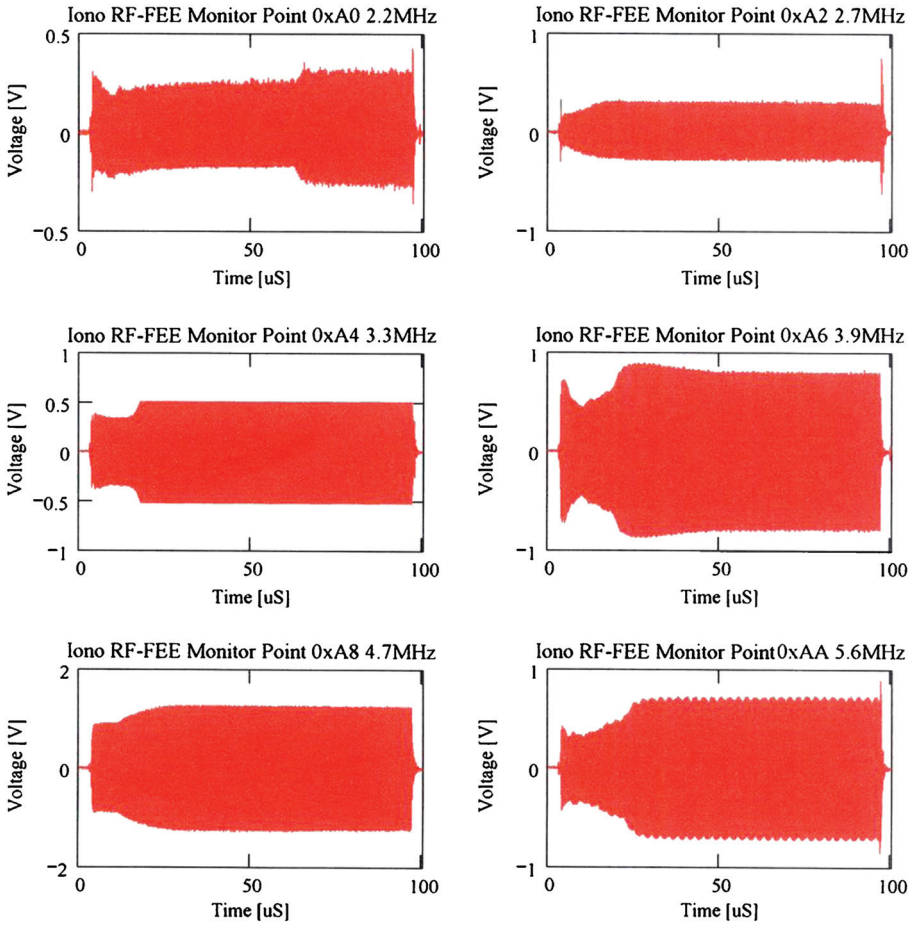


**Figure 6.** Evolution of the sounding wave amplitude on the MARSIS antenna measured in the engineering laboratory and captured on an oscilloscope for six values of the sounding frequency. At all frequencies, the wave is at greater than 1/2 amplitude by 3 μs after the impulse commences.

to noise or interference. If the trace is done visually, this step will be incorporated into the data-taking procedure.

[24] The somewhat coarse resolution of the time delay measurements implies that the plot of delay time versus sounding frequency will have a quantized, or stair-step, appearance to it. Although this irregularity is not a serious impediment to a useful inversion of the ionospheric trace, it is marginally more precise to smooth out these results. There are various algorithms for performing this operation; however, since it is not considered essential, we do not include such an algorithm here. Again, this step is only necessary if the data are taken by an automated procedure; a person using a visual method can effectively smooth the result by eye.

## 6. The Inversion Routine

[25] The purpose of the previous four sections is to acquire a reliable value of the time delay as a function of the sounding frequency. The resulting function can then be inverted to get the profile of electron density as a function of altitude. The process makes a number of assumptions: propagation along the nadir direction, plane parallel stratification of the ionosphere, nonmagnetic plasma dispersion relation, and that the profile is monotonic.

[26] The condition of propagation along the nadir direction is known to be violated in the case of structures in the ionosphere associated with cusp regions between crustal magnetic structures [*Duru et al.*, 2006; *Nielsen et al.*, 2007]. More recent work by *Duru et al.* [2010b] indicates that off-nadir propagation may affect the ionospheric trace more commonly than is currently supposed; however, of the four assumptions listed, the most commonly violated in an obvious way is the last, the assumption that the electron density profile is monotonic above the ionospheric peak. Cusps are often visible in the ionospheric trace at low sounding frequencies and altitudes much higher than the peak [see, e. g., *Kopf et al.*, 2008; *Wang et al.*, 2009]. Figure 7, from *Kopf et al.* [2008], shows an example of a cusplike ionospheric trace. In these cases, specialized methods, such as those of *Zou et al.* [2010], are needed to reliably invert the trace. In this manual, we will only deal with the simplest case, in which the physical profile can reasonably be assumed to be monotonic.

[27] The integral equation to be inverted is given by

$$\tau_i = 2 \times \int_{z_0}^{z_i} \frac{dz}{V_g} = 2 \times \int_{z_0}^{z_i} \frac{dz}{c\sqrt{1 - \left(\frac{f_{pe}(z)}{fs,i}\right)^2}} \qquad (2)$$

where the group velocity, from the dispersion relation for propagation of an electromagnetic wave in a nonmagnetic plasma, is given by the denominator of the right-hand side

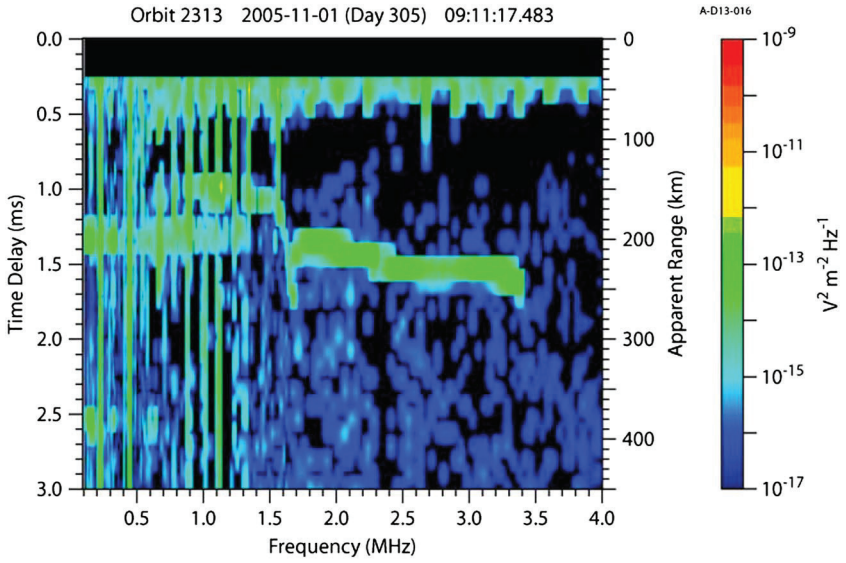


**Figure 7.** Ionogram showing cusplike nonmonotonic ionospheric trace. The cusp can be seen near frequency 1.6 MHz and between time delays of 1.3 and 1.8 ms.

of equation (2). In equation (2), $z$ stands for the range from the spacecraft in the nadir direction. The factor of 2 is present because the sounding wave traverses the range between spacecraft and reflector in both directions. The subscript $i$ indexes the sounding frequency, so that $\tau_i$ stands for the delay time measured for the sounding frequency $f_{s,i}$. Equation (2) must be solved for the $z_i$, the range from the spacecraft to the reflection point for the $i$th sounding frequency.

[28] The solution to equation (1) can be carried out in a number of ways. The classical solution is called Abel's transformation and yields the solution

$$z(f_n) = \frac{2}{\pi}\int_{\alpha_0}^{\pi/2} \frac{c}{2}\tau(f_n \sin\alpha)d\alpha \tag{3}$$

where $f_n$ is the frequency for which we wish to compute the range from the spacecraft and $sin(\alpha_0)$ is equal to $f_0/f_n$. A derivation of equation (3) using Laplace transforms is given by *Manning* [1947]. A slightly different derivation is given by *Budden* [1961]. In this formulation, $f_n$ and $\tau$ are thought of as continuous functions. The profile of $\tau$ as a function of $f_n$ can easily be converted to a continuous function and equation (2) then solved; however, it is usually more convenient to skip this step by solving equation (2) by explicitly assuming a functional form for $f_{pe}(z)$ and stepwise solving equation (2) over discrete intervals in $z$. Because this method involves solution layer-by-layer, it is called the "lamination" method. We shall discuss this method of solution next.

[29] Thorough outlines of the application of the classic lamination method—widely used in the analysis of ground-based ionograms—to MARSIS topside sounding ionograms, can be found in papers by *Zou and Nielsen* [2004], *Nielsen et al*. [2006], *Morgan et al*. [2008], and *Zou et al*. [2010]. The general lamination method is also discussed in the classic text by *Rishbeth and Garriott* [1969], with references therein enumerating several variations on the process, including the approach adopted here. *Jackson* [1969] gives a detailed account of inversion of terrestrial topside ionograms. The following development follows that of *Morgan et al*. [2008], which is simplified from that of *Jackson* [1969]. The process of *Morgan et al*. [2008] differs from that of *Jackson* [1969] primarily because at Mars there is negligible effect from the magnetic field, eliminating the need for iteration of the integral. In addition, *Morgan et al*. [2008] use "linear-in-log $n$" rather than the "parabolic-in-log $n$" because the gains from enforcing continuous derivatives at lamination boundaries do not justify the added complication. Attempting to enforce smooth derivatives at the lowest frequency reflection point can cause ringing of the solution with consequent unphysical results. Therefore, the method preferred here is the simple linear-in-log $n$ lamination method.

[30] The lamination method involves dividing the ionosphere into plane parallel strata at the points where data are taken. If we compute the integral for the $i$th data point, then we are integrating from the zeroth point (i. e., the position of the spacecraft) to data point $i$. The ray path integral can be rewritten as a sum

$$\tau_{\text{delay},i} = \sum_{j=1}^{i} \Delta\tau_{\text{delay},i,j} = \frac{2}{c}\sum_{j=1}^{i}\int_{z_{j-1}}^{z_j} \frac{dz}{\sqrt{1-\left(\frac{f_{pe}(z)}{f_{s,i}}\right)^2}} \tag{4}$$

where the index $i$ refers to the total time delay $\tau_{\text{delay},i}$ corresponding to sounding frequency $f_{s,i}$, $f_{pe}$ is the variable of integration corresponding to the value of the plasma frequency at a position along the ray path, the index $j$ refers to the interval along the ray path corresponding to sounding frequency interval $f_{s,j-1} < f_{pe} \le f_{s,j}$ where $1 \le j \le i$.

[31] The two commonly used functional forms assumed for the values of $f_{pe}(z)$ in the denominator of equation (3) are linear and exponential. Solution involving the linear form is discussed by, e. g., *Rishbeth and Garriott* [1969] and *Zou and Nielsen* [2004]. The exponential form is used by *Morgan et al*. [2008] and *Zou et al*. [2010]. Where the data points are very close together, the two methods are virtually equivalent; however, because the form of the electron density profile in the large gap between the spacecraft position and the first reflection point is thought on average to be of exponential

form, we here give that version. This allows the investigator to use a single process to compute the whole profile rather than finding an exponential for the first segment and the linear formulation for the rest. Aside from this matter of convenience, neither method has an advantage over the other.

[32] Using the exponential form for the $j$th subinterval, from data point $j-1$ to data point $j$, we assume that the plasma frequency has the form

$$f_{\mathrm{pe}}(z) = f_{s,j-1}\exp(\alpha_j z) \tag{5}$$

which can be inverted to

$$z = \frac{1}{\alpha_j}\ln\frac{f_{\mathrm{pe}}}{f_{s,j-1}} \tag{6}$$

where $\alpha_j$ is the exponential growth constant for the ray path corresponding to frequency interval $f_{\mathrm{s},j-1} \le f_{\mathrm{pe}} \le f_{\mathrm{s},j}$. This relation enables us to change variables from $z$ to $f_{\mathrm{pe}}$ in the individual $j$ terms of equation 4:

$$\Delta\tau_{\mathrm{delay},i,j} = \frac{2}{c}\int_{f_{\mathrm{pe},j-1}}^{f_{\mathrm{pe},j}} \frac{df_{\mathrm{pe}}}{\alpha_j f_{\mathrm{pe}}\left[1-\left(f_{\mathrm{pe}}/f_{s,i}\right)^2\right]^{1/2}} \tag{7}$$

If we make the further change of variable $f_{\mathrm{pe}}/f_{\mathrm{s},i} = \sin\theta$, then the $j$th term of the $i$th delay time becomes

$$\Delta\tau_{\mathrm{delay},i,j} = \frac{2}{c}\int_{\theta_{i,j-1}}^{\theta i,j} \frac{1}{\alpha_j f_{s,j}\sin\theta}\frac{f_{s,j}\cos\theta d\theta}{\cos\theta} = \frac{2}{\alpha_j c}\int_{\theta_{i,j-1}}^{\theta i,j}\frac{d\theta}{\sin\theta} \tag{8}$$

where

$$\theta_{i,j} = \arcsin\left(f_{s,j}/f_{s,i}\right) \tag{9}$$

The integral in Equation (8) can be computed by elementary methods to get

$$\Delta\tau_{\mathrm{delay},i,j} = \frac{1}{c\alpha_j}\ln\frac{\left[1-\sqrt{1-\left(f_{s,j}/f_{s,i}\right)^2}\right]\left[1+\sqrt{1-\left(f_{s,j-1}/f_{s,i}\right)^2}\right]}{\left[1-\sqrt{1-\left(f_{s,j-1}/f_{s,i}\right)^2}\right]\left[1+\sqrt{1-\left(f_{s,j}/f_{s,i}\right)^2}\right]} \tag{10}$$

or, using Equation 9,

$$\Delta\tau_{\mathrm{delay},i,j} = \frac{1}{c\alpha_j} ln\frac{\left[1-\cos\theta_{i,j}\right]\left[1+\cos\theta_{i,j-1}\right]}{\left[1+\cos\theta_{i,j}\right]\left[1-\cos\theta_{i,j-1}\right]} \tag{11}$$

[33] This form can be made even more compact using trigonometric identities [*Zou et al.*, 2010]. Because the $f_{\mathrm{s},j}$'s are just the sounding frequencies intermediate between the spacecraft, index 0, and the desired data point $i$, everything in this expression is either a measured time delay or a fixed frequency except the exponential coefficients $\alpha_j$. If we insert the terms of Equation (10) into Equation (4), we find

$$\tau_{\mathrm{delay},i} = \sum_{j=1}^{j=i}\frac{1}{c\alpha_j}\ln\frac{\left[1-\sqrt{1-\left(f_{s,j}/f_{s,i}\right)^2}\right]\left[1+\sqrt{1-\left(f_{s,j-1}/f_{s,i}\right)^2}\right]}{\left[1-\sqrt{1-\left(f_{s,j-1}/f_{s,i}\right)^2}\right]\left[1+\sqrt{1-\left(f_{s,j}/f_{s,i}\right)^2}\right]} \tag{12}$$

[34] If there are $n$ sounding frequencies, then this set of equation constitutes a linear system of $n$ equations in $n$ variables $\alpha_j$. The system can be efficiently solved by starting with $i=1$, solving for $\alpha_1$, and using this value in the $i=2$ equation, proceeding through $i=n$. A piece of Interactive Data Language (IDL) code that has been found useful is included below.

```
    pro range_exp_comp,freq_arr_mhz,time_arr_msec,range_exp

   c_kmps=3.e5

n_freqs=n_elements(freq_arr_mhz)

range_exp=dblarr(n_freqs)

alpha_arr=dblarr(n_freqs)
freq_rat=dblarr(n_freqs,n_freqs)

diff_exp=dblarr(n_freqs,n_freqs)

freq_arr=freq_arr_mhz*1e6

l_rat_freq=alog(freq_arr(1:*)/freq_arr)

time_arr=(time_arr_msec)*1e-3/2.0

time_arr(0)=0.

app_range=c_kmps*time_arr

for i=1,n_freqs-1 do begin

freq_rat(i,0:i)=freq_arr(0:i)/freq_arr(i)

endfor

freq_rat=asin(freq_rat)

for i=1,n_freqs-1 do begin

freq_rat(i,i)=!dpi/2.d0

endfor

cos_f=cos(freq_rat)

exp_weight=0.5*alog((1.d0-cos_f)/(1.d0+cos_f))

for i=1,n_freqs-1 do begin

diff_exp(i,1:i)=exp_weight(i,1:i)-exp_weight(i,0:i-1)

endfor

alpha_arr(1)=-diff_exp(1,1)/app_range(1)

for i=2,n_freqs-1 do begin

alpha_arr(i)=-diff_exp(i,i)/ $

(app_range(i)+total((diff_exp(i,1:i-1)/alpha_arr(1:i-1))))

endfor

range_exp(0)=0.0d0

for i=1,n_freqs-1 do begin

range_exp(i)=range_exp(i-1)-l_rat_freq(i-1)/alpha_arr(i)

endfor
```

[35] Inputs are freq_arr_mhz, the sampled frequencies in MHz, and time_arr_msec, measured delay times in ms. The output is range_exp, computed range from the spacecraft in kilometers. The spacecraft altitude is needed to compute the altitude. The zeroth element of freq_arr_mhz should be the spacecraft-local plasma frequency, or an estimate if it is unavailable. The zeroth element of time_arr_msec should be 0. The effect of using Equation (8) on the trace shown in Figure 1 is shown in Figure 8. The red trace in this figure shows the data points as taken from the ionospheric trace shown by the dashed line in Figure 9. The black trace is the electron density profile, corrected for dispersion using Equation 10 represented by the code shown above.

## 7. Comparison With a Radio Occultation Profile and Some Caveats

[36] To illustrate consistency of our method with a process that is completely independent, we here compare a series of MARSIS AIS electron density profiles with a publicly available trace from the MARSIS Radio Science experiment aboard Mars Express. In Figure 9, we compare a Mars Express Radio Science (MaRS) electron density profile from MEX orbit 4253, shown as a solid dark blue curve, with a number of comparable profiles computed from MARSIS AIS traces, shown in red. The MARSIS AIS traces are solid in the frequency range where reflected waves are observed; they are shown as dashed lines in the gap between the spacecraft-local data point and the lowest-frequency sounding echo. Table 1 gives various ephemeris quantities of the MaRS profile and the several comparable MARSIS AIS profiles. We were able to find several MARSIS AIS profiles whose solar zenith angle is close to that of the MaRS profile, at 66° solar zenith angle (SZA); however, we were unable to simultaneously match other important parameters such as the latitude, solar longitude (that is, season), and local time. This problem occurs for two reasons: (1) by design, MaRS and MARSIS cannot operate simultaneously, and (2) the viewing geometries of the two experiments are at odds with each other: MARSIS AIS does remote sensing ideally in the nadir direction while MaRS must view the ionosphere at grazing incidence to the planet with the radio wave directed at Earth, a much more restrictive condition. Even though the conditions are not the same for latitude, solar longitude, and local time, Figure 9 shows that in the frequency range where MARSIS AIS detects the reflected wave, the results of the two experiments are consistent.

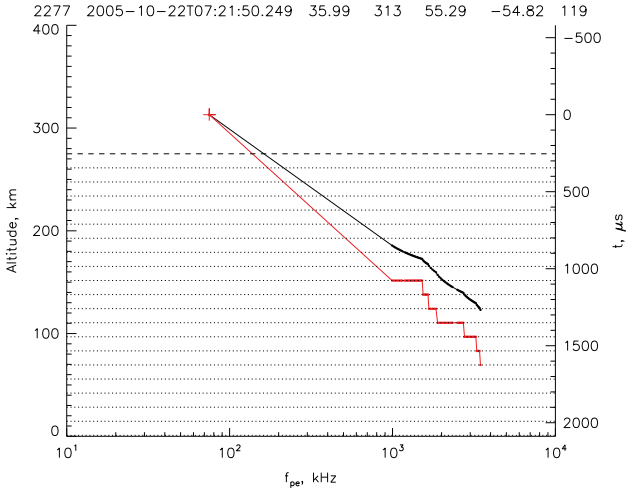


**Figure 8.** Inversion of Figure 1. The red points give the apparent altitude from the ionogram. The black points are the inversion using the algorithm given in Section 6.

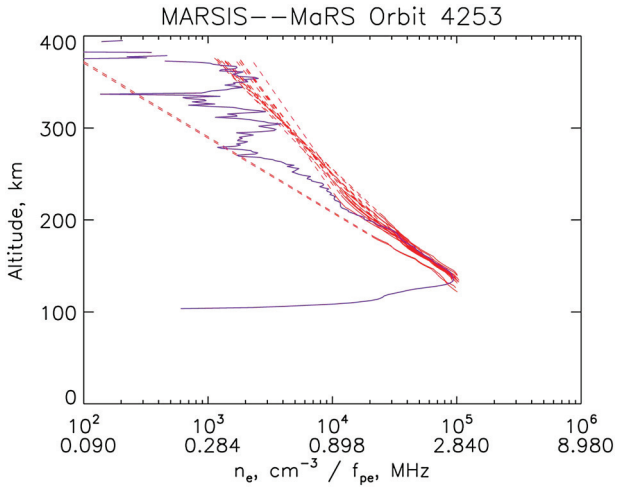


**Figure 9.** Comparison of a Mars Express Radio Science electron density profiles with several comparable MARSIS AIS profiles.

**Table 1.** Comparison data for MaRS Orbit 4253 EDP and MARSIS AIS Comparables

| EDP Source | Orbit | SZA (deg) | Lat (deg) | $L_{solar}$ (deg) | E. Long. (deg) | LTST (h) |
|---|---|---|---|---|---|---|
| MaRS | 4253 | 66.29 | 42.57 | 227.81 | 45.50 | 10.07 |
| MARSIS AIS | 7544 | 64.20 | 68.88 | 12.78 | 278.28 | 12.74 |
| MARSIS AIS | 7544 | 63.75 | 68.40 | 12.78 | 278.44 | 12.75 |
| MARSIS AIS | 7544 | 63.30 | 67.92 | 12.78 | 278.61 | 12.76 |
| MARSIS AIS | 7544 | 62.85 | 67.45 | 12.78 | 278.77 | 12.78 |
| MARSIS AIS | 7544 | 62.40 | 66.97 | 12.78 | 278.91 | 12.79 |
| MARSIS AIS | 7544 | 61.95 | 66.49 | 12.78 | 279.04 | 12.80 |
| MARSIS AIS | 7544 | 61.50 | 66.01 | 12.78 | 279.18 | 12.81 |
| MARSIS AIS | 7544 | 61.05 | 65.53 | 12.78 | 279.32 | 12.82 |
| MARSIS AIS | 7548 | 63.71 | 68.65 | 13.33 | 235.01 | 12.71 |
| MARSIS AIS | 7548 | 63.26 | 68.17 | 13.33 | 235.18 | 12.72 |
| MARSIS AIS | 7548 | 62.81 | 67.70 | 13.33 | 235.34 | 12.73 |
| MARSIS AIS | 7548 | 62.35 | 67.22 | 13.33 | 235.48 | 12.74 |
| MARSIS AIS | 7548 | 61.90 | 66.74 | 13.33 | 235.62 | 12.76 |
| MARSIS AIS | 7548 | 61.45 | 66.26 | 13.33 | 235.76 | 12.77 |
| MARSIS AIS | 7581 | 61.87 | 68.96 | 17.86 | 146.74 | 12.38 |
| MARSIS AIS | 7581 | 61.40 | 68.48 | 17.86 | 146.91 | 12.39 |

LTST, Local True Solar Time.

[37] Examination of Figures 1, 4, and 5, as well as Figure 9 reveals the weakest link in the electron density profile acquisition process: the large frequency gap between the spacecraft-local plasma frequency measurement and the first sounding point. The reason for this recurring data gap is twofold: (1) the strength of the sounding wave decreases sharply at low frequency, a characteristic of transmission from a dipole antenna, and (2) plasma frequency harmonics and other noise often obscure the ionospheric trace. Either of these conditions can make the ionospheric trace impossible

to discern at frequencies below about 1.5 MHz. As explained in the previous section, the solution of all practitioners so far has been to assume an exponential fall-off in density with increasing altitude. This appears to be a good assumption on average. The work of [*Duru et al*., [2008], using statistical analysis of the local plasma frequency measurements over a wide range of altitudes and solar zenith angles bears out the assumption of exponential decrease with altitude. This is not a complete solution for two reasons. First, *Duru et al*. [2008] showed that, when the spacecraft is outside the ionosphere and in the shocked solar wind, the harmonics on which the local plasma frequency is based are usually not available. In these cases, one must make a reasonable assumption about the electron density at the spacecraft. Second, the plasma densities sampled by *Duru et al*. [2008] were at altitudes well above the main layer, where the scale height is much greater than that close to the peak density of the main layer. In traces where MARSIS does not sample to low enough frequencies, the assumption of an exponential decrease with height leads to a false interpolation in scale height. In these cases, the scale height in the important region just above the main layer is calculated to be too small, leading to the altitude of the ionospheric layer being calculated as too high.

[38] Although the low frequency data gap is a real problem, it should also be borne in mind that, to some extent, the inversion process is self correcting. Equation (1) shows that the correction for dispersion becomes vanishingly small as the sounding frequency becomes much larger than the plasma frequency of the medium through which it is traveling. Thus, the dispersion correction is largely due to plasma in the vicinity of the reflection point. If the frequency range of the reflected trace is much larger than the gap between the spacecraft-local measurement and the first sounding point, the error in the trace will be small and confined to the region around the first sounding point.

[39] With these considerations, we conclude that electron density profiles may be unreliable if taken at spacecraft altitudes that are too high (typically over 800 km) or where the frequency interval in which sounding echoes are visible is less than the interval between the spacecraft plasma frequency and the lowest-frequency sounding point. This latter condition applies for virtually any trace taken on the night side or near the terminator down to solar zenith angles of about 85°. Methods for dealing with the problems of short sampling intervals and high altitudes are currently under development.

[40] As emphasized previously, another area for caution is that a sounder cannot get a reflection from under a shelf or overhang in the plasma density. It is for this reason that the X-ray induced "M1" layer at 90–100 km altitude is rarely detected by MARSIS; it exists at altitudes below the main ionospheric layer and almost never exceeds it in density. As discussed in Section 4 and documented by *Kopf et al*. [2008], cusplike features in the plasma density are often visible at higher altitudes, indicating that there is a shelf or overhang in the ionospheric structure. The inversion process as outlined in Section 4 cannot take these structures into account. Procedures for partially inverting this type of structure are outlined by *Budden* [1961]. More recently, *Zou et al*. [2010] present a fitting method explicitly tailored for such profiles.

[41] MARSIS AIS is a surprisingly versatile instrument that has yielded new ionospheric science at Mars. Local density measurements have been used independently to characterize the Martian ionosphere by *Duru et al*. [2008]. The combination of MARSIS AIS local electron densities and ASPERA-3 plasma measurements has proven fruitful in describing the solar wind—ionosphere boundary [*Duru et al*., 2010a; *Dubinin et al*., 2008]. MARSIS AIS electron density profiles, based on ionospheric traces combined with local densities, were first used *en mass* to characterize the Martian ionosphere by *Morgan et al*. [2008]. This work was extended by *Němec et al*. [2011], who used local densities at high altitude and electron density profiles around the ionospheric peak to create a comprehensive model of the dayside Martian ionosphere. In addition, we have not, in this paper, touched on implications of the ability of MARSIS AIS to measure the local magnetic field strength. *Duru et al*. [2006], *Akalin et al*. [2010], and *Morgan et al*. [2011] are examples of the utility of this measurement. To sum up, the variety of measurements available and the sheer volume of data ensure that MARSIS Active Ionospheric Sounding will provide insights into the Martian ionosphere for some time to come.

[42] **Acknowledgments.** This research was supported by NASA through contract 1224107 with the Jet Propulsion Laboratory. The first author would like to thank several members of the Mars Upper Atmosphere Network (MUAN) for reading and commenting on the manuscript. We thank Dr. Mike Terkildsen for independently verifying the correct operation of the code included in this paper. Mars Express Radio Science (MaRS) data were downloaded from the ESA Planetary Science Archive, at www.rssd.esa.int/psa/MARS–EXPRESS/MRS/MEX–M–MRS–5–OCC–9101–V2.0/DATA/$OCC_1ONO/2007/DOY_1 18_4 253_2 007$.

## References

Akalin, F., D. D. Morgan, D. A. Gurnett, D. L. Kirchner, D. A. Brain, R. Modolo, M. H. Acuña, and J. R. Espley (2010), Dayside induced magnetic field in the ionosphere of Mars, *Icarus*, *206*, 104–111, doi:10.1016/j.icarus.2009.03.021.

Benson, R. F. (1985), Field-aligned electron density irregularities near 500 km: Equator to polar cap topside sounder observations, *Radio Sci.*, *20*(3), 477–485.

Benson, R. F. (2008), Plasma physics using space-borne radio sounding, in *Radio Sounding and Plasma Physics*, CP974, edited by P. Song, J. Foster, M. Mendillo, and D. Bilitza, p. 2033, American Institute of Physics, doi:10.1063/1.2885028.

Benson, R. F. (2010), Four decades of space-borne radio sounding, *Radio Sci. Bull.*, (333), 24–44.

Benson, R. F., and D. Bilitza (2009), New satellite mission with old data: Rescuing a unique data set, *Radio Sci.*, *44*, RS0A04, doi:10.1029/2008RS004036.

Budden, K. G. (1961), *Radio Waves in the Ionosphere*, Cambridge University Press, New York.

Décréau, P. M. E., et al. (2001), Early results from the Whisper instrument on cluster: An overview, *Ann. Geophys.*, *19*, 1241–1258.

Dubinin, E., et al. (2008), Structure and dynamics of the solar wind/ionosphere interface on Mars: MEX-ASPERA-3 and MEX-MARSIS observations, *Geophys. Res. Lett.*, *113*, L11103, doi:10.1029/2008GL033730.

Duru, F., D. A. Gurnett, T. F. Averkamp, D. L. Kirchner, R. L. Huff, A. M. Persoon, J. J. Plaut, and G. Picardi (2006), Magnetically controlled structures in the ionosphere of Mars, *J. Geophys. Res.*, *111*, A12204, doi:10.1029/2006JA011975.

Duru, F., D. A. Gurnett, D. D. Morgan, R. Modolo, A. F. Nagy, and D. Najib (2008), Electron densities in the upper ionosphere of Mars from the excitation of electron plasma oscillations, *J. Geophys. Res.*, *113*, A07302, doi:10.1029/2008JA013073.

Duru, F., D. A. Gurnett, J. D. Winningham, R. A. Frahm, and R. Modolo (2010a), A plasma flow velocity boundary at Mars from the disappearance of electron plasma oscillations, *Icarus*, *206*, 74–82, doi:10.1016/j.icarus.2009.04.012.

Duru, F., D. D. Morgan, and D. A. Gurnett (2010b), Overlapping iononspheric and surface echoes observed by the Mars Express radar

sounder near the Martian terminator, *Geophys. Res. Lett.*, *37*, L23102, doi:10.1029/2010GL045859.
Franklin, C. A., and M. A. Maclean (1969), The design of swept-frequency topside sounders, *Proc. IEEE*, *57*(6), 897–929.
Gurnett, D. A., et al. (2004), The cassini radio and plasma wave investigation, *Space Sci. Rev.*, *114*, 395–463, doi:10.1007/s11214-004-1434-0.
Gurnett, D. A., et al. (2005), Radar soundings of the ionosphere of Mars, *Science*, *310*, 1929–1933, doi:10.1126/science.1121868.
Jackson, J. E. (1969), The reduction of topside ionograms to electron-density profiles, *Proc. IEEE*, *57*, 960–975.
Jordan, R., et al. (2009), The Mars Express MARSIS sounder instrument, *Planet. Space Sci*, *57*, 1975–1986, doi:10.1016/j.pss.2009.09.016.
Kopf, A. J., D. A. Gurnett, D. D. Morgan, and D. L. Kirchner (2008), Transient layers in the topside ionosphere of Mars, *Geophys. Res. Lett.*, *35*, L17102, doi:10.1029/2008GL034948.
Manning, L. A. (1947), The determination of ionospheric electron distribution, *Proc. IEEE*, *35*, 1203–1207.
McAfee, J. R. (1969), Topside resonances as oblique echoes, *J. Geophys. Res., Space Phys.*, *74*, 802–808.
Morgan, D. D., D. A. Gurnett, D. L. Kirchner, J. L. Fox, E. Nielsen, and J. J. Plaut (2008), Variation of the Martian ionospheric electron density from Mars Express radar soundings, *J. Geophys. Res.*, *113*, A09303, doi:10.1029/2008JA013313.
Morgan, D. D., D. A. Gurnett, F. Akalin, D. A. Brain, J. S. Leisner, F. Duru, R. A. Frahm, and J. D. Winningham (2011), Dual-spacecraft observation of large-scale magnetic flux ropes in the Martian ionosphere, *J. Geophys. Res.*, *116*, A02319, doi:10.1029/2010JA016134.
Muldrew, D. B. (1972), Electron resonances observed with topside sounders, *Radio Science*, *7*, 779–789.
Němec, F., D. D. Morgan, D. A. Gurnett, F. Duru, and V. Truhlik (2011), Day-side ionosphere of Mars: Empirical model based on data from the MARSIS instrument, *J. Geophys. Res.*, *116*, E107003, doi:10.1029/2010JE003789.
Nielsen, E., et al. (2006), Observations of vertical reflections from the topside Martian ionosphere, *Space Science Rev.*, doi:10.1007/s11214-006-9113-y.
Nielsen, E., X.-D. Wang, D. A. Gurnett, D. L. Kirchner, R. Huff, R. Orosei, A. Safaeinili, J. J. Plaut, and G. Picardi (2007), Vertical sheets of dense plasma in the topside Martian ionosphere, *J. Geophys. Res.*, *112*, E02003, doi:10.1029/2006JE002723.
Reinisch, B. W. (1996), Modern ionosondes, in *Modern Ionospheric Science*, edited by H. Kohl, R. Rüster, and K. Schlegel, pp. 440–458, European Geophysical Society.
Rishbeth, H., and O. K. Garriott (1969), *Introduction to Ionospheric Physics*, pp. 331, Academic Press: New York.
Schunk, R. W., and A. F. Nagy (2000), *Ionospheres: Physics*, Plasma Physics, and Chemistry, Cambridge University Press, New York.
Wang, M. Y., and J. S. Ping (2012), Martian ionogram scaling by the Object Tracking Method, *Sci. China: Phys. Mech. Astron.*, *55*(3), 540–545, doi:10.1007/s11433-012-4639-3.
Wang, X.-D., J.-S. Wang, E. Nielsen, and H. Zou (2009), "Hook" structure in MARSIS ionogram and its interpretation, *Geophys. Res. Lett.*, *36*, L13103, doi:10.1029/2009GL038844.
Zou, H., and E. Nielsen (2004), Methods for obtaining electron density profiles from MARSIS ionograms and derivation of parameters characterizing the profiles, max-Planck-Institüt internal document MPAe-W-485-04-01.
Zou, H., E. Nielsen, J.-S. Wang, and X.-D. Wang (2010), Reconstruction of nonmonotonic electron density profiles of the Martian topside ionosphere, *Planet. Space Sci.*, *58*(10), 1391–1399, doi:10.1016/j.pss.2010.06.011.